

Coexistence Analysis of H2H and M2M Traffic in FiWi Smart Grid Communications Infrastructures Based on Multi-Tier Business Models

Martin Lévesque, Frank Aurzada, Martin Maier, *Senior Member, IEEE*, and Géza Joós *Fellow, IEEE*

Abstract—In this paper, we study the performance of multi-tier integrated fiber-wireless (FiWi) smart grid communications infrastructures based on low-cost, simple, and reliable next-generation passive optical network (PON) with quality-of-service (QoS) enabled wireless local area networks (WLANs) in terms of capacity, latency, and reliability. We study the coexistence of human-to-human (H2H), e.g., triple-play traffic, and machine-to-machine (M2M) traffic originating from wireless sensors operating on a wide range of possible configurations. Our analysis enables the quantification of the maximum achievable data rates of both event- and time-driven wireless sensors without violating given upper delay limits of H2H traffic. By using experimental measurements of real-world smart grid applications we investigate the impact of variable H2H traffic loads on the sensor end-to-end delay performance. The obtained results show that a conventional Ethernet PON may cause a bottleneck and increase the delay for both H2H and M2M traffic. In contrast, by using a 10G-EPON or wavelength division multiplexing (WDM) PON the bottleneck arises in the wireless network. Furthermore, we study the interplay between time- and event-driven nodes and show that the theoretical upper bound of time-driven sensors decreases linearly as a function of the number of sensors, while with event-driven sensors the upper bound decrease is nonlinear and more pronounced.

I. INTRODUCTION

THE communications requirements of a wide range of potential smart grid applications have been recently quantified in terms of latency, bandwidth, reliability, and security [1]. The authors concluded that a *fast* and *reliable* smart grid communications infrastructure is necessary to enable real-time exchange of data among distributed elements. Although IEEE P2030 opted for a technology agnostic approach and thus doesn't specify any communications technologies of choice, it is favorable to rely on the exceptionally low-latency characteristics of fiber optic facilities and wireless technologies, where fiber is available to some but not all points in the system [2].

In this paper, we focus on integrated fiber-wireless (FiWi) smart grid communications infrastructures based on next-generation Ethernet passive optical network (EPON) and wireless local area network (WLAN) technologies. EPON combines the low cost and simplicity of Ethernet equipment with the completely passive (i.e., unpowered) network infrastructure of PONs, which render them inherently highly reliable. Beside legacy EPON, we explore the benefits of emerging high-speed time division multiplexing (TDM) PONs and multi-channel wavelength channel multiplexing (WDM) PONs of

extended fiber reach, which represent the most promising candidates of next-generation optical access networks [3]. On the wireless side, we deploy quality-of-service (QoS) enabled high-throughput WLANs with service differentiation among multiple traffic classes as well as with emerging very high throughput (VHT) enhancements.

More importantly, we pay particular attention to the fact that business models, arguably more than technological choices, play a key role in the roll-out of smart grid communications infrastructures. According to [4], utilities along with municipalities are responsible for 22% of households passed with fiber-to-the-building/home (FTTB/H) in Europe. These investments enable utilities and/or municipalities to (i) leverage their existing duct, sewer, and other infrastructure, (ii) create a new source of revenue in the face of ongoing liberalization of the energy sector, particularly in smart grids solutions, and (iii) provide services completely independent from incumbents' infrastructures. Furthermore, it was recently shown in [5] that cooperation among different utilities in the roll-out phase may drive down the capital expenditures (CAPEX) of FTTB/H deployments by 17%. Innovative partnerships enable utilities and other players to share smart grid communications infrastructures investments by transitioning from the traditional vertical network integration model towards splitting the value chain into a three-tier business model that consists of network infrastructure roll-out, network operation/maintenance, and service provisioning [4].

The objectives of this paper are as follows. We aim at providing deeper insights into the performance of multi-tier FiWi communications networks that are installed, operated, and maintained by a single or multiple utilities and provide not only open-access triple-play service offerings, also known as human-to-human (H2H) services, but also enable the support of some of the aforementioned potential smart grid applications, e.g., grid integration of renewable energy resources [6]. The unpredictability of renewable energy sources, in conjunction with other emerging and future smart grid applications such as grid-to-vehicle/vehicle-to-grid (G2V/V2G), creates challenging problems in the control and reliability of the power grid, which call for a multitude of geographically and temporally coordinated monitoring and control actions over time scales ranging from milliseconds to operational planning horizon [7]. Towards this end, different wireless sensor applications based on ZigBee or low-power WLAN technologies have been considered for the machine-to-machine (M2M) interconnection of a wide variety of devices

This work was supported by the FQRNT MERIT Short-term Research Scholarship Program and NSERC Strategic Project Grant No. 413427-2011.

and appliances, giving rise to the so-called Internet of Things (IoT) [8], of which the smart grid represents an important real-world example. Practical deployment guidelines in terms of “safe distance” and “safe offset frequency” for the interference avoidance of coexisting ZigBee and WLAN networks for smart grid applications were developed in [9]. In this paper, however, we investigate the coexistence of H2H and M2M traffic over integrated FiWi smart grid communications infrastructures based on next-generation EPON and WLAN technologies by means of probabilistic analysis in terms of capacity, latency, and reliability. According to the IEEE P2030 standard, the main quality attributes of the customer and distribution domains of the communications technology interoperability architectural perspective (CT-IAP) of smart grids are latency and reliability. On another note, the access network should be energy efficient, but it is important to note that the main goal of smart grids is to use advanced communications networks to improve the efficiency of the underlying power grid. In this paper, our goal is to quantify the maximum achievable wireless sensor traffic rates without resulting detrimental impact on the latency performance of conventional H2H traffic, which can be used as a theoretical upper bound of coexisting M2M traffic for the realization of emerging and future yet unforeseen smart grid applications.

The main contributions of this paper are as follows:

- Probabilistic modeling of time- and event-driven smart grid sensors integrated with regular WLAN stations and next-generation PONs allowing the calculation of the end-to-end delay, throughput, and reliability.
- Algorithm for finding the theoretical upper bounds of M2M traffic for a given H2H delay threshold. The upper bounds may be used to set the maximum sensor data rate.
- Fine-grained investigation of different FiWi settings using experimental measurements of smart grid applications based on IEC Standard 61850:
 - Impact of varying H2H traffic for different PON flavors.
 - Sensibility analysis of interplay between time- and event-driven nodes.
- The analytical framework may also be used for the proper dimensioning and planning of shared FiWi smart grid communications infrastructures: using the topology, MAC settings, and traffic load as inputs, the model is able to provide the main network performance metrics as outputs. It may be extended by including economical costs in order to compare the expected network performance with required operating costs, giving rise to a powerful network design tool.

The remainder of the paper is structured as follows. The FiWi smart grid communications infrastructures and wireless sensors under consideration are described in Section II. Their coexistence performance under H2H and M2M traffic is analyzed in Section III. Section IV presents numerical and verifying simulation results. Section V concludes the paper.

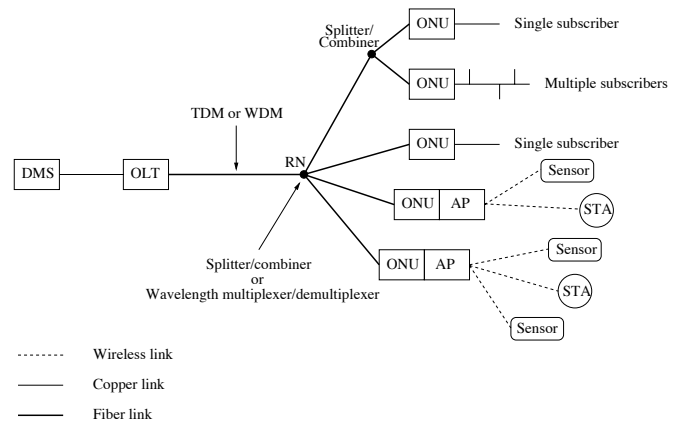


Fig. 1. Generic architecture of integrated FiWi smart grid communications infrastructures.

II. FIWI SMART GRID COMMUNICATIONS INFRASTRUCTURES

Fig. 1 depicts the generic architecture of our considered FiWi smart grid communications infrastructures. The fiber backhaul consists of an EPON with its typical tree-and-branch topology. The central optical line terminal (OLT) is located at the root of the fiber tree and connects to the distribution management system (DMS) of the underlying power distribution network. Optical networks units (ONUs), the EPON customer premises equipment, are attached to the fiber tree leaf nodes. An ONU either directly serves a single or multiple subscribers or hosts a collocated WLAN access point (AP) with associated wireless sensors and stations (STAs).

More specifically, the fiber backhaul may be built by using a legacy IEEE 802.3ah EPON, which uses a time-shared downstream wavelength channel and another separate time-shared upstream wavelength channel, each operating at a data rate of 1 Gb/s. The remote node (RN) consists of an optical power splitter/combiner. In the upstream direction, bandwidth is dynamically assigned to individual ONUs by the OLT based on a report-grant mechanism. Alternatively, high-speed 10+ Gb/s TDM PONs or wavelength-broadcasting/routing WDM PONs may be used. IEEE 802.3av 10G-EPON offers higher symmetric and asymmetric data rates of up to 10 Gb/s, but is otherwise similar to EPON. A wavelength-broadcasting WDM PON leaves the splitter/combiner at the RN in place and deploys multiple wavelength channels. Each of these wavelength channels is broadcast to all connected WDM upgraded ONUs and is used for bidirectional transmission. Each WDM ONU is able to select a wavelength by using a tunable bandpass filter and reuses the downstream modulated signal coming from the OLT for upstream data transmission by means of remodulation techniques. In the case of a wavelength-routing WDM PON, the splitter/combiner at the RN is replaced with a wavelength multiplexer/demultiplexer such that each of the WDM wavelength channels on the common feeder fiber is routed to a different distribution fiber. A given wavelength channel may be dedicated to a single ONU (e.g., business subscriber) or be time shared by multiple wavelength-independent ONUs (e.g., residential subscribers). Finally, long-reach WDM PONs with

an extended optical range of up to 100 km may be used to achieve major cost savings by consolidating optical access and aggregation networks.

Each AP forms a separate WLAN zone that comprises its associated STAs and sensors. Each WLAN uses Enhanced Distributed Channel Access (EDCA), specified in IEEE 802.11e, for QoS support. EDCA provides QoS-enabled STAs with service differentiation by employing four different access categories (ACs), each having a different arbitration inter-frame space (AIFS), a different minimum and maximum contention window CW_{min} and CW_{max} , respectively, and a different maximum channel holding time per traffic class. Apart from conventional IEEE 802.11 a/b/g/n WLANs with raw data rates in the range of 54-600 Mb/s, we also consider emerging IEEE 802.11ac VHT WLAN technologies that exploit physical layer enhancements to achieve raw data rates of up to 6900 Mb/s.

As for the wireless sensors, it is expected that beside raw data rates of 12 kb/s for basic voltage and current sensors, computed quantities (i.e., phase amplitude, phase angle, sequence components, etc.) will increase the bandwidth requirements to about 200-500 kb/s, or up to 2-5 Mb/s for millisecond sampling in rapid fault detection systems [2]. They may operate at various cycles, including cycles as low as 10 or 100 milliseconds, to estimate critical system parameters [7]. The wireless sensors may be conventional ZigBee devices, offering low data rates of up to 250 kb/s, or may use advanced IEEE 802.15.4 compliant signaling schemes to support variable data rates between 31.25 kb/s and 2 Mb/s [10]. Alternatively, to reuse existing WLAN infrastructures and thus allow for key cost savings and faster deployments, emerging low-power sensors based on IEEE 802.11 technology may be used for periodic or event-triggered data transmissions [8].

For improved security, the various PONs and WLANs may apply IEEE standard 802.1AE and 802.11i, respectively, in conjunction with the aforementioned standards.

III. COEXISTENCE ANALYSIS

Recently, the first FiWi analytical framework was developed in [11] to evaluate the performance of integrated PONs and WLAN IEEE 802.11n/ac routing algorithms without taking any wireless sensors and service differentiation into account. In this work, the focus is on the wireless front-end for the integration of wireless sensors, while the fiber backhaul is assumed to be the same as in [11].

Our analysis builds on the recently proposed novel methodology to model the QoS performance of WLANs using EDCA [12]. To gain insights into the performance of wireless sensors coexisting with conventional STAs, we extend the methodology by incorporating the *inhomogeneous* and *non-saturated* cases, where WLAN nodes can be either wireless sensors or STAs and which might be non-saturated, i.e., they must not constantly have frames to send. Furthermore, we extend the analysis to the generalized case of *multiple* traffic classes, where each WLAN node is equipped with multiple queues for different traffic classes rather than a single one.

Furthermore, the analysis developed in this work accommodates both event- and time-driven sensors. In the case of event-driven sensors, all sensors compete for channel access using

TABLE I
MAIN SYMBOLS OF THE COEXISTENCE ANALYSIS.

Symbol	Description
L	Average generated frame size in bps.
C	Set of traffic classes. For each class c , $c \in C$.
\mathcal{N}	Set of FiWi nodes, corresponding to a total of one OLT, O ONUs, and N wireless nodes, $ \mathcal{N} = 1 + O + N$.
S_{ij}	Average number of frames generated from FiWi node $i \in \mathcal{N}$ destined to FiWi node $j \in \mathcal{N}$.
$\lambda_{i,c}^{wi}$	Average number of frames generated by the wireless node i of class c .
D^d, D^u	Downstream and upstream average PON delays, respectively.
D_{TDM}	Transmission time of time-driven sensors.
E	Average cycle duration of event-driven wireless nodes.
P_{succ}	Probability that the cycle ends with a successful transmission.
T_{succ}, T_{coll}	Average time of a successful transmission and collision, respectively.
$W_{k,c,s}$	Contention window value of queue c at wireless network node k in backoff stage s .
$\Pi_{k,c}(s, j)$	Steady-state probability that queue c of node k is in the backoff stage s with backoff counter value j , for the case when there is at least one frame waiting for transmission.
$\Pi_{k,c}(0, j, 0)$	Steady-state probability for the case when there is no frame waiting for transmission.
$q_{k,c}$	Probability that there is a frame in queue c of node k at the beginning of a cycle.
$p_{k,c}$	Collision probability in any time slot of a frame of class c from node k .
$D_{k,c}^{wi}$	Total wireless delay experienced by a frame in queue c of node k for both time- and event-driven nodes.
D_c	Average end-to-end delay of traffic class c .
\mathcal{R}_c	End-to-end probabilistic reliability of traffic class c .

EDCA, whereby time-driven sensors have dedicated periodic channel access. For convenience, Table I summarizes the main symbols and their description used in our coexistence analysis.

A. Network Model

The PON consists of one OLT and O attached ONUs. The TDM PON carries one upstream wavelength channel and a separate downstream wavelength channel. We suppose that both the wavelength-broadcasting and the wavelength-routing WDM PONs carry Λ bidirectional wavelength channels $\lambda = 1, \dots, \Lambda$. In the wavelength-routing WDM PON, the O ONUs are divided into Λ sectors. We use λ to index the wavelength channel as well as the corresponding sector. In our model, sector λ , $\lambda = 1, \dots, \Lambda$, accommodates O_λ ONUs. Specifically, ONUs with indices o between $\sum_{v=1}^{\lambda-1} O_v$ and $\sum_{v=1}^{\lambda} O_v$ belong to sector λ . Thus, sector $\lambda = 1$ comprises ONUs $o \in \mathcal{S}_1 = \{1, \dots, O_1\}$, sector $\lambda = 2$ comprises ONUs $o \in \mathcal{S}_2 = \{O_1 + 1, \dots, O_1 + O_2\}$, and so on, while we assign the index $o = 0$ to the OLT. The one-way propagation delay between OLT and ONUs of sector λ is $\tau^{(\lambda)}$ (in seconds) and the data rate of the associated wavelength channel λ is denoted by $\mathcal{C}^{(\lambda)}$ (in bit/s). Hence, each sector of the wavelength-routing WDM PON is allowed to operate at a different data rate serving a subset of ONUs located at a different distance from the OLT (e.g., business vs. residential service areas). For ease of exposition, we assume that in the wavelength-broadcasting TDM and WDM PONs all wavelength channels operate at the same data rate \mathcal{C} (in bit/s) and that all ONUs have the one-

way propagation delay τ (in seconds) from the OLT. All or a subset of the O ONUs are equipped with an AP to interface with wireless sensors and STAs. The WLAN is assumed to operate at data rate r (in bit/s).

B. Traffic Model

We denote \mathcal{N} for the set of FiWi smart grid communications infrastructure nodes that act as traffic sources and destinations. Specifically, we consider \mathcal{N} to contain the OLT, the O ONUs, and a given number of \tilde{N}_s wireless sensors and \tilde{N}_r STAs, totalling $\tilde{N} = \tilde{N}_s + \tilde{N}_r$ wireless nodes. Hence, the number of traffic sources/destinations is given by $|\mathcal{N}| = 1 + O + \tilde{N}$. We define the traffic matrix $\mathbf{S} = (S_{ij})$, $i, j \in \mathcal{N}$, where S_{ij} represents the number of frames per second that are generated at source node i and destined to node j ($S_{ij} = 0$ for $i = j$). We allow for any arbitrary distribution of the frame length L and denote \bar{L} and $Var(L)$ for the mean and variance of the length of each generated frame, respectively. The traffic generation is assumed to be ergodic and stationary.

Inter-ONU communications can be done only via the OLT, i.e., there is no direct communication among ONUs, neither optically nor wirelessly. However, each ONU equipped with an additional AP is able to directly communicate with its associated wireless sensors and STAs. For communications with the remaining wireless sensors and STAs, a given ONU has to send traffic to the corresponding ONU serving the destination wireless sensor or STA. Taking these communications rules (or routing) into account, one can determine the amount of traffic in the optical and wireless parts for each pair of source node i and destination node j of a given traffic matrix \mathbf{S} . Specifically, let Γ_{ij} denote the number of frames per second to be sent between ONUs and OLT across the fiber infrastructure, whereby i and j may be any the O ONUs or the OLT. Furthermore, let $\lambda_{i,c}^{wi}$ denote the number of frames per second to be sent from queue c of any wireless network node i , whereby i may be any of the \tilde{N} wireless sensors and STAs or their associated AP with collocated ONU.

C. Stability and Capacity Analysis

1) *Fiber Backhaul*: For the wavelength-routing WDM PON, we define the downstream traffic intensity in sector λ , $\lambda = 1, \dots, \Lambda$, as follows [11, Eq. (2)]:

$$\rho^{d,\lambda} = \frac{\bar{L} \cdot R^{d,\lambda}}{\mathcal{C}(\lambda)}, \quad (1)$$

while the upstream traffic intensity is given by [11, Eq. (4)]

$$\rho^{u,\lambda} = \frac{\bar{L} \cdot R^{u,\lambda}}{\mathcal{C}(\lambda)}. \quad (2)$$

$R^{d,\lambda}$ and $R^{u,\lambda}$ represent the downstream and upstream traffic rates of wavelength λ and were derived in [11, Eqs. (2-4)]. For stability, the normalized downstream and upstream traffic intensities have to satisfy $\rho^{d,\lambda} < 1$ and $\rho^{u,\lambda} < 1$, respectively [11, Eq. (5)].

Note that $R^{d,\lambda}$ and $R^{u,\lambda}$ account for the traffic coming from both the wireless and optical networks. For the wireless case of event-driven nodes when the retransmission limit is

reached, one needs to consider only successfully transmitted frames, that is, $\lambda_{i,c}^{wi} \cdot r_{i,c}^{wi}$, where $r_{i,c}^{wi}$ represents the probabilistic reliability (to be derived shortly).

In the case of the wavelength-broadcasting TDM PON ($\Lambda = 1$) and WDM PON ($\Lambda > 1$), the normalized downstream traffic rate (intensity) ρ^d and normalized upstream traffic rate (intensity) ρ^u are derived as in [11, Eqs. (6-7)]. The wavelength-broadcasting TDM and WDM PONs work stable if $\rho^u < 1$ and $\rho^d < 1$.

2) *Wireless Front-end*: The wireless front-end comprises the \tilde{N} wireless sensors and STAs as well as the subset of ONUs equipped with an AP, which we refer to as the wireless network nodes. The queue c at wireless network node i is stable if

$$D_{i,c}^{wi,a} < \frac{1}{\lambda_{i,c}^{wi}}, \quad (3)$$

where $D_{i,c}^{wi,a}$ denotes the average access delay of queue c of node i to the wireless channel (to be calculated shortly in Section III-D). For stability, the normalized traffic rate (intensity) $\rho_{i,c}$ at queue c of wireless network node i has to satisfy

$$\rho_{i,c} = D_{i,c}^{wi,a} \cdot \lambda_{i,c}^{wi} < 1. \quad (4)$$

The subsequent delay analysis of Section III-D applies only for a stable network. Note that we consider a stable operating system for which Eqs. (3) and (4) hold. Stability can be ensured in practical setups through admission control.

D. Delay Analysis

1) *Fiber Backhaul*: In the wavelength-routing WDM PON, the OLT sends a downstream frame to an ONU in sector λ by transmitting the frame on wavelength λ , which is received by all ONUs in the sector. We model all downstream transmissions in sector λ to emanate from a single queue as in [11].

Weighing the downstream delays $D^{d,\lambda}$ in the different sectors λ by their relative downstream traffic intensities $\rho^{d,\lambda} / \sum_{\lambda=1}^{\Lambda} \rho^{d,\lambda}$ yields the average downstream delay of the wavelength-routing WDM PON [11, Eq. (10)]:

$$D^d = \frac{1}{\sum_{\lambda=1}^{\Lambda} \rho^{d,\lambda}} \sum_{\lambda=1}^{\Lambda} \rho^{d,\lambda} \cdot D^{d,\lambda}. \quad (5)$$

For the upstream delay, we model each wavelength channel λ , $\lambda = 1, \dots, \Lambda$, as a single upstream wavelength channel of a conventional EPON. The average upstream delay of the wavelength-routing WDM PON equals [11, Eq. (12)]:

$$D^u = \frac{1}{\sum_{\lambda=1}^{\Lambda} \rho^{u,\lambda}} \sum_{\lambda=1}^{\Lambda} \rho^{u,\lambda} \cdot D^{u,\lambda}. \quad (6)$$

Next, the average downstream (D^d) and upstream delays (D^u) for the wavelength-broadcasting TDM PON ($\Lambda = 1$) and WDM PON ($\Lambda > 1$) can be calculated using [11, Eqs. (16-17)].

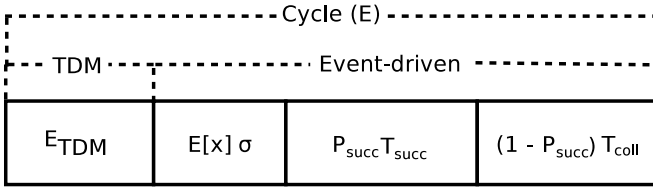


Fig. 2. Channel access cycle to model both time-/event-driven sensor and STA transmissions.

2) *Wireless Front-end*: Similar to [12], time is divided into cycles, however each cycle consists of four components (rather than 3 in [12]): (i) average time division multiplexing (TDM) duration for time-based sensors (ii) a randomly chosen time interval for contention resolution on the wireless channel, followed by (iii) one successful transmission or collision, as depicted in Fig 2. In contrast to [12], however, in each cycle typically only a subset of the wireless network nodes compete for channel access, while the others do not have any frames waiting in their queues to be sent (i.e., non-saturated case).

Each wireless node is assumed to have C queues, one per traffic class under consideration. Each separate queue c , $c = 1, \dots, C$, is assigned a priority in ascending order from $c = 1$ to $c = C$. Let $W_{k,c,s}$ denote the contention window value of queue c at wireless network node k in backoff stage s , where $s = 0, 1, \dots, R_{k,c}$, and $R_{k,c}$ is the given retry limit of queue c at node k . Furthermore, let $B_{k,c}(i)$ be the steady-state probability that queue c of wireless node k has backoff counter value i at the beginning of a cycle, where $0 \leq i \leq \max_{s=0,1,\dots,R_{k,c}} W_{k,c,s}$ (to be computed shortly). For notational convenience, similarly to [12, Eq. (3)], we define

$$\beta_{k,c}(i) = \begin{cases} 0 & i \leq 0 \\ \sum_{j=0}^{i-1} B_{k,c}(j) & i > 0 \\ 1 & i > \max_{s=0,1,\dots,R_{k,c}} W_{k,c,s}, \end{cases} \quad (7)$$

where $\beta_{k,c}(i)$ denotes the steady-state probability that queue c 's backoff counter at node k has expired at backoff slot i in a cycle. Moreover, let $\delta_{k,c} \geq 0$ be an integer denoting the minimum number of backoff slots, in addition to its assigned AIFS number, queue c of node k has to wait until accessing the wireless channel, whereby $\delta_{k,c} = 0$ represents the minimum waiting time, i.e., DIFS plus zero backoff slots.

Next, we define $q_{k,c}$ as the probability that there is a frame in queue c of node k at the beginning of a cycle (to be calculated shortly). Let then $Q_{h,c}(i)$ denote the probability that from wireless network node h 's perspective no competing node transmits before backoff slot i . The calculation of $Q_{h,c}(i)$ is different from [12] in that we extend it to multiple classes per node and also include the case that no frame may be in the queues of other wireless network nodes (non-saturated case). Consequently, using our above introduced backlog probability $q_{k,c}$ we obtain

$$Q_{h,c}(i) = \prod_{k \neq h} \prod_{z=1}^C [(1 - q_{k,z}) + q_{k,z}(1 - \beta_{k,z}(i - \delta_{k,z}))] \cdot \prod_{z < c} [(1 - q_{h,z}) + q_{h,z}((1 - \beta_{h,z}(i - \delta_{h,z})) +$$

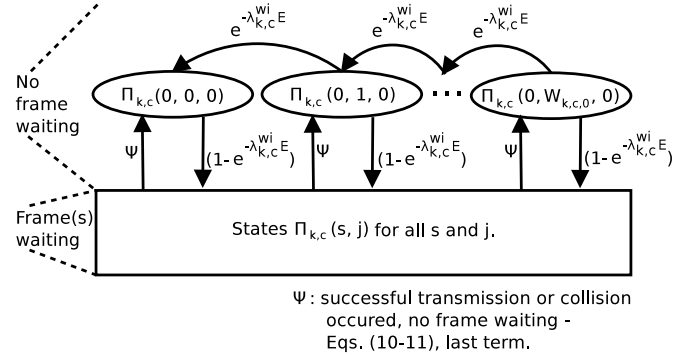


Fig. 3. Steady-state probabilities of the backoff counter value evolution in the EDCA model under non-saturated conditions.

$$\beta_{h,z}(i - \delta_{h,z}) \beta_{h,c}(i - \delta_{h,c})) \cdot \prod_{z > c} [(1 - q_{h,z}) + q_{h,z}(1 - \beta_{h,z}(i - \delta_{h,z}))]. \quad (8)$$

Adopting a notation similar to [12], the probability $T_{h,c}(i)$ that queue c of wireless network node h sees the first transmission in a cycle exactly at backoff slot i is defined as [12, Eq. (5)].

To derive the steady-state probability that queue c of node k is in backoff stage s with backoff counter value j , we have to define the following probabilities in order to account for the possibility that there are no frames waiting for transmission at node k , represented in the lower part in Fig. 3. Let

$$\Pi_{k,c}(s, j), \quad \begin{aligned} s &\in \{0, 1, \dots, R_{k,c}\} \\ j &\in \{0, 1, \dots, W_{k,c,s}\} \end{aligned} \quad (9)$$

be the probability that node k has a frame waiting in its queue c , is in backoff stage s , and has backoff counter value j . By extending Eq. (12) in [12] to the multiple-queue per node case, we obtain for $0 < s \leq R_{k,c}$ and $0 \leq j \leq W_{k,c,s}$

$$\begin{aligned} \Pi_{k,c}(s, j) &= \Pi_{k,c}(s, j)(1 - Q_{k,c}(\delta_{k,c})) \\ &+ \sum_{r=1}^{W_{k,c,s-j}} \Pi_{k,c}(s, j+r) \cdot T_{k,c}(r-1 + \delta_{k,c}) \\ &+ \sum_{i=1}^{W_{k,c,s-1}} \left[\Pi_{k,c}(s-1, i) \cdot T_{k,c}(i + \delta_{k,c}) \cdot \frac{1}{W_{k,c,s} + 1} \right]. \end{aligned} \quad (10)$$

Contrary to Eq. (13) in [12], however, for $s = 0$ and $0 \leq j \leq W_{k,c,s}$ we have

$$\begin{aligned} \Pi_{k,c}(0, j) &= \Pi_{k,c}(0, j)(1 - Q_{k,c}(\delta_{k,c})) \\ &+ \sum_{r=1}^{W_{k,c,0-j}} \Pi_{k,c}(0, j+r) \cdot T_{k,c}(r-1 + \delta_{k,c}) \\ &+ \sum_{i=0}^{W_{k,c,R_{k,c}}} q_{k,c} \left[\Pi_{k,c}(R_{k,c}, i) \cdot T_{k,c}(i + \delta_{k,c}) \right] \end{aligned}$$

$$\begin{aligned} & \cdot \frac{1}{W_{k,c,0} + 1} \Big] + \sum_{s=0}^{R_{k,c}} \sum_{i=0}^{W_{k,c,s}} q_{k,c} \left[\Pi_{k,c}(s, i) \cdot \right. \\ & \left. Q_{k,c}(i + 1 + \delta_{k,c}) \cdot \frac{1}{W_{k,c,0} + 1} \right] \\ & + \Pi_{k,c}(0, j, 0) \cdot \left(1 - e^{-\lambda_{k,c}^{wi} E} \right), \end{aligned} \quad (11)$$

where E denotes the average duration of a cycle in steady state (to be calculated shortly) and $\Pi_{k,c}(0, j, 0)$ is the newly defined probability (represented in the upper part in Fig. 3) that node k has no frame in its queue c (and therefore is in backoff stage 0) and has backoff counter value j , $j \in \{0, 1, \dots, W_{k,c,0}\}$, which is given by

$$\begin{aligned} \Pi_{k,c}(0, j, 0) &= \sum_{i=0}^{W_{k,c,R_{k,c}}} \left[\Pi_{k,c}(R_{k,c}, i) \cdot T_{k,c}(i + \delta_{k,c}) \cdot \right. \\ & \left. \frac{1 - q_{k,c}}{W_{k,c,0} + 1} \right] + \sum_{s=0}^{R_{k,c}} \sum_{i=0}^{W_{k,c,s}} \left[\Pi_{k,c}(s, i) \cdot \right. \\ & \left. Q_{k,c}(i + 1 + \delta_{k,c}) \cdot \frac{1 - q_{k,c}}{W_{k,c,0} + 1} \right] \\ & + \Pi_{k,c}(0, j + 1, 0) \cdot e^{-\lambda_{k,c}^{wi} E}. \end{aligned} \quad (12)$$

After computing $\Pi_{k,c}(s, j)$ and $\Pi_{k,c}(0, j, 0)$, we are now able to compute the above defined probability $B_{k,c}(i)$ that queue c of wireless node k has backoff counter value j , $0 \leq j \leq \max_{s=0,1,\dots,R_{k,c}} W_{k,c,s}$, at the beginning of a cycle as follows (extension of [12, Eq. (6)]):

$$B_{k,c}(j) = \sum_{s=0}^{R_{k,c}} \Pi_{k,c}(s, j) + \Pi_{k,c}(0, j, 0). \quad (13)$$

Next, let us calculate the probability that node k had a successful transmission in a cycle, provided that it had a frame waiting in its queue c , which is similar to [12, Eq. (16)] and given by

$$P_{succ}(k, c) = \sum_{i=0}^{W_{k,c,max}} B_{k,c}(i) \cdot Q_{k,c}(i + 1 + \delta_{k,c}), \quad (14)$$

where $W_{k,c,max}$ is the maximum contention window size of node k 's queue c and $B_{k,c}(i)$ denotes the steady-state probability that queue c of node k has backoff counter value i . The probability that the cycle ends with a successful transmission is then given by

$$P_{succ} = 1 - \prod_{\forall k} \prod_{\forall c} [1 - P_{succ}(k, c)]. \quad (15)$$

This in turn allows us now to compute the average duration of a cycle. In our calculation, we consider both *event-driven* and *time-driven sensors*. Event-driven sensors contend for channel access like any other STA after detecting an event of importance, e.g., power outage. Conversely, time-driven sensors periodically send their measurements to the DMS in dedicated (contention-free) TDM slots without undergoing contention for the wireless channel. Extending [12, Eq. (17)],

the average cycle duration is given by

$$\begin{aligned} E &= E_{TDM} \\ &+ \mathbb{E}[x] \cdot \sigma \\ &+ P_{succ} \cdot T_{succ} + (1 - P_{succ}) \cdot T_{coll}, \end{aligned} \quad (16)$$

where E_{TDM} is the mean channel access time due to a contention-free period consisting of periodically recurring TDM slots for time-driven sensors in a given zone z . It is approximated by

$$E_{TDM} = P_{TDM,z} \cdot (T_{succ} + D_{TDM}), \quad (17)$$

whereby $P_{TDM,z}$ denotes the probability that a wireless node has to wait due to a TDM slot in a given zone z , which is given by

$$\begin{aligned} P_{TDM,z} &= \sum_{\forall s \text{ sensors}} \lambda_{s,sen}^{wi} \cdot D_{TDM} \\ &+ \frac{1}{(1/(\sum_{\forall s \text{ sensors}} \lambda_{s,sen}^{wi} - D_{TDM}))/T_{succ}} \end{aligned} \quad (18)$$

with

$$\begin{aligned} D_{TDM} &= \text{PHY Header} + \text{MAC Header}/r \\ &+ \mathbb{E}[\text{Payload}] + \text{FCS}/r + \delta. \end{aligned} \quad (19)$$

Note that $P_{TDM,z}$ defines the interplay between cycles and TDM slots, whereby the transmissions of contending wireless nodes are highly influenced by the recurring TDM slots of time-driven sensors. Also note that $P_{TDM,z} = 0$ (and thus $E_{TDM} = 0$) if all sensors in zone z are event driven.

Furthermore, σ denotes the duration of one time slot, while T_{succ} and T_{coll} represent the average time of a successful transmission and collision, respectively. The calculation of T_{succ} and T_{coll} depends on the access mechanism in place (basic access or RTS/CTS access mechanism) and can be done in a straightforward fashion following the approach in [13], whereby DIFS needs to be replaced with the minimum AIFS after a successful transmission and with EIFS after a collision. For instance, under the assumption of the RTS/CTS access mechanism, collisions can occur only on RTS frames and we thus have

$$\begin{aligned} T_{succ} &= \text{RTS}/r + \text{SIFS} + \delta + \text{CTS}/r + \text{SIFS} + \delta \\ &+ \text{PHY Header} + \text{MAC Header}/r \\ &+ \mathbb{E}[\text{Payload}] + \text{FCS}/r + \text{SIFS} + \delta + \text{ACK}/r \\ &+ \text{AIFS} + \delta \end{aligned} \quad (20)$$

and

$$T_{coll} = \text{RTS}/r + \text{EIFS} + \delta, \quad (21)$$

where δ denotes the propagation delay and $\mathbb{E}[\text{Payload}]$ is the average transmission time of a frame, which is equal to \bar{L}/r . (Note that in IEEE 802.11 the parameters RTS, CTS, and ACK as well as the MAC Header and FCS are given in bits, while the other parameters are given in seconds.)

Extending [12, Eq. (20)] to the nodal multiple-queue case, we obtain the second expectation in Eq. (16) as

$$\mathbb{E}[x] = \sum_{j=1}^{\max_{k,c}(W_{k,c,max} + \delta_{k,c})} Q_0(j), \quad (22)$$

with

$$Q_0(j) = \prod_{\forall k} \prod_{\forall c} [1 - \beta_{k,c}(j - \delta_{k,c})]. \quad (23)$$

Furthermore, we can also calculate the above defined probability $q_{k,c}$ that there is a frame in queue c of node k at the beginning of a cycle. Clearly, we have

$$\begin{aligned} q_{k,c} &= 1 - Pr[\text{no frame waiting in queue } c \\ &\quad \text{of node } k \text{ after a cycle}] \\ &= 1 - \left[(1 - q_{k,c}) \cdot \left(1 - \frac{1 - e^{-\lambda_{k,c}^{wi} E}}{1 - P_{TDM,z}} \right) \right. \\ &\quad \left. + q_{k,c} \cdot P_{succ}(k, c) \right]. \end{aligned} \quad (24)$$

By solving Eq. (24) for $q_{k,c}$ we obtain

$$q_{k,c} = \frac{(1 - e^{-\lambda_{k,c}^{wi} E}) / (1 - P_{TDM,z})}{(1 - e^{-\lambda_{k,c}^{wi} E}) / (1 - P_{TDM,z}) + P_{succ}(k, c)}. \quad (25)$$

Next, we calculate the average access delay of wireless nodes, including event-driven sensors, which comprises two delay components. The first delay component, $D_{k,c}^{sen}$, is experienced when a given node senses the wireless channel busy with probability P_z^{wait} without gaining successful channel access (with probability $1 - P_{succ}(k, c)$). In this event, the node waits until the end of the transmission and then enters backoff stage 0. Thus, we have

$$D_{k,c}^{sen} = P_z^{wait} \cdot (1 - P_{succ}(k, c)) \cdot \left(T_{succ} + \frac{W_{k,c,0}}{2} \sigma \right) \quad (26)$$

with

$$P_z^{wait} = \frac{\sum_k EDCA \text{ node} \in z \sum_c \lambda_{k,c}^{wi}}{1/T_{succ}}. \quad (27)$$

The probability P_z^{wait} is approximated by the ratio of the traffic load and the maximum achievable load $1/T_{succ}$. The second delay component is the average backoff and contention time period $D_{k,c}^{back}$ of queue c at node k and is obtained as

$$\begin{aligned} D_{k,c}^{back} &= \sum_{s=1}^{R_{k,c}} (p_{k,c})^s \cdot (1 - p_{k,c}) \cdot \\ &\quad \left[s \left(T_{coll} + \delta_{k,c} \sigma + P_z^{wait} \cdot (1 - P_{succ}(k, c)) \right) \right. \\ &\quad \left. \cdot T_{succ} \right) + \left(\sum_{j=1}^s \frac{W_{k,c,j}}{2} \right) \sigma \right], \end{aligned} \quad (28)$$

whereby the collision probability in any given time slot, similar to Eq. (24) in [12], is defined as

$$p_{k,c} = \sum_{i=0}^{W_{k,c,max} + \delta_{k,c}} \frac{T_{k,c}(i)}{Q_{k,c}(i)}. \quad (29)$$

Note that in Eq. (28), the delay at each stage s is characterized by the collision duration, $\delta_{k,c}$, sensing duration, and backoff duration.

The average access delay $D_{k,c}^{wi,a}$ for a frame successfully transmitted from queue c of wireless node k is the sum of the aforementioned two delay components plus successful transmission and is equal to

$$D_{k,c}^{wi,a} = D_{k,c}^{sen} + D_{k,c}^{back} + \frac{T_{succ}}{P_{succ}(k, c)}. \quad (30)$$

By taking also the queuing delay into account, we obtain the total wireless delay experienced by a frame in queue c of node k for both time- and event-driven nodes as follows:

$$D_{k,c}^{wi} = \begin{cases} \frac{1}{1/D_{k,c}^{wi,a} - \lambda_{k,c}^{wi}}, & \text{for event-driven nodes.} \\ D_{TDM}, & \text{for time-driven nodes.} \end{cases} \quad (31)$$

3) *End-to-End Delay*: In this section, we compute the average end-to-end delay across both the fiber backhaul and wireless front-end. We distinguish the two cases of (i) regular H2H traffic (e.g., triple-play voice, video, and data traffic) and (ii) sensor M2M traffic.

- **Regular H2H traffic**: The average end-to-end delay for regular traffic class c , $c = 1, \dots, C$, is given by

$$\begin{aligned} D_c &= \frac{1}{\sum_{\forall i,j \in \mathcal{N} \setminus \{\text{Sensors}\}} S_{ij}} \left[\sum_{\substack{\forall \text{ STAs } i,j \\ \text{or ONU/AP } j \\ \text{in same zone}}} S_{ij} \cdot D_{i,c}^{wi} \right. \\ &\quad + \sum_{\forall \text{ STA } i} S_{i0} (D_{i,c}^{wi} + D^u) \\ &\quad + \sum_{\substack{\forall \text{ STA } i \\ \text{and ONU/AP } j \\ \text{in other zones}}} S_{ij} (D_{i,c}^{wi} + D^u + D^d) \\ &\quad + \sum_{\substack{\forall \text{ STA } i \\ \text{and STA } j \\ \text{in other zones}}} S_{ij} (D_{i,c}^{wi} + D^u + D^d + \\ &\quad \quad \quad D_{\text{ONU/AP } j,c}^{wi}) \\ &\quad + \sum_{\forall \text{ ONU } i} S_{i0} \cdot D^u + \sum_{\forall \text{ ONUs } i,j} S_{ij} (D^u + D^d) \\ &\quad + \sum_{\substack{\forall \text{ ONU } i \\ \text{and STA } j \\ \text{in other zones}}} S_{ij} (D^u + D^d + D_{\text{ONU/AP } j,c}^{wi}) \\ &\quad + \sum_{\forall \text{ ONU } j} S_{0j} \cdot D^d \\ &\quad \left. + \sum_{\forall \text{ STA } j} S_{0j} (D^d + D_{\text{ONU/AP } j,c}^{wi}) \right], \end{aligned} \quad (32)$$

where D^d represents the average PON downstream delay and D^u represents the average PON upstream delay.

- **Sensor M2M traffic:** The average end-to-end delay for sensor traffic class c , $c = 1, \dots, C$, is given by

$$\begin{aligned}
 D_c = & \frac{1}{\sum_{\substack{\forall \text{ sensor } i \\ \text{and OLT,} \\ \text{ONUs, STAs } j}} S_{ij}} \left[\sum_{\forall \text{ sensor } i} D_{i,c}^{wi} \cdot \sum_{\substack{\forall \text{ STAs } j \\ \text{in same zone}}} S_{ij} \right. \\
 & + \sum_{\forall \text{ sensor } i} S_{i0} (D_{i,c}^{wi} + D^u) \\
 & + \sum_{\substack{\forall \text{ sensor } i \\ \text{and ONU } j \\ \text{in other zones}}} S_{ij} (D_{i,c}^{wi} + D^u + D^d) \\
 & \left. + \sum_{\substack{\forall \text{ sensor } i \\ \text{and STA } j \\ \text{in other zones}}} S_{ij} (D_{i,c}^{wi} + D^u + D^d + \right. \\
 & \left. D_{\text{ONU/AP } j,c}^{wi}) \right]. \quad (33)
 \end{aligned}$$

E. Reliability

We define reliability as the probability Θ_s that a sensor transmits frames successfully within the retry limit:

$$\Theta_s = \begin{cases} \mathcal{R}_c & \text{for event-driven sensors,} \\ 1 & \text{for time-driven sensors,} \end{cases} \quad (34)$$

where

$$\begin{aligned}
 \mathcal{R}_c = & \frac{1}{\sum_{\substack{\forall \text{ sensor } i \\ \text{and OLT,} \\ \text{ONUs, STAs } j}} S_{ij}} \left[\sum_{\forall \text{ sensor } i} r_{i,c}^{wi} \cdot \sum_{\substack{\forall \text{ STAs } j \\ \text{in same zone}}} S_{ij} \right. \\
 & + \sum_{\forall \text{ sensor } i} S_{i0} \cdot r_{i,c}^{wi} + \sum_{\substack{\forall \text{ sensor } i \\ \text{and ONU } j \\ \text{in other zones}}} S_{ij} \cdot r_{i,c}^{wi} \\
 & \left. + \sum_{\substack{\forall \text{ sensor } i \\ \text{and STA } j \\ \text{in other zones}}} S_{ij} \cdot r_{i,c}^{wi} \cdot r_{\text{ONU/AP } j,c}^{wi} \right], \quad (35)
 \end{aligned}$$

with

$$r_{i,c}^{wi} = 1 - (p_{i,c})^{R_{i,c}+1}. \quad (36)$$

F. Theoretical Upper Bound of Permissible M2M Traffic

In order to find the theoretical upper bound of permissible M2M traffic without violating a given delay limit of H2H traffic, the sensor data rate, $\lambda_{i,c}^{wi}$, needs to be iteratively increased until the regular traffic delay reaches the delay limit. Assuming a delay limit of \mathcal{L}_r , we find the theoretical upper bound of permissible M2M traffic iteratively by using the following *max* function:

$$\text{max}_{l \in [0..\infty]} (\lambda_{\forall i,c}^{wi} := l), D_c < \mathcal{L}_r, \quad (37)$$

where c denotes a regular traffic class and i indicates a sensor. By increasing the sensor data rate and updating the model for D_c iteratively, the maximum sensor data rate not violating the given delay limit of H2H traffic is obtained.

G. Future Modeling Improvements

In this section, we outline further steps that might be required to render our model more accurate for practical settings. First, in the wireless domain, no bit-error-ratio (BER) at the physical layer was considered. The BER modeling approach proposed in [11, Eq. (24)] can be adapted to capture physical impairments. Note that BER in the optical domain can be considered negligible.

Furthermore, in the presented analytical model, we consider that all sensors can reach an AP directly. However, in certain sensor applications we might need to install new sensors on-the-fly without direct access to an AP. Assuming that smart grid sensors are typically static, the WLAN model can be extended to a multi-hop wireless mesh network with IEEE 802.11s support following a similar modeling approach as presented in [11, Eq. (39)].

Also, from a practical perspective, the obtained numerical results should be compared with real-world measurements. The resultant performance differences, if any, can be used to further improve the accuracy of our proposed analytical framework.

IV. NUMERICAL AND SIMULATION RESULTS

A. Configurations

The EDCA parameters are set to the default values given in [12] and frames are first assumed to have a size of 1500 bytes. STAs, ONUs, and OLT send unicast H2H traffic at rate α_r uniformly distributed among each other with $\delta_{k,c} = 3$, $CW_{min} = 64$, and $CW_{max} = 256$. Sensor M2M traffic at rate $\lambda_{i,c}^{wi}$ is destined to the DMS with $\delta_{k,c} = 0$, $CW_{min} = 8$, and $CW_{max} = 256$. The traffic matrix can therefore be described as follows, whereby source nodes are listed vertically and destination nodes horizontally:

$$\begin{matrix}
 & & 0 & \dots & O + \tilde{N}_r & \dots & O + \tilde{N}_r + \tilde{N}_s \\
 0 & & \left(\begin{array}{cccccc}
 0 & \alpha_r & \alpha_r & 0 & 0 \\
 \alpha_r & \alpha_r & \alpha_r & 0 & 0 \\
 \alpha_r & \alpha_r & 0 & 0 & 0 \\
 \lambda_{i,c}^{wi} & 0 & 0 & 0 & 0 \\
 \lambda_{i,c}^{wi} & 0 & 0 & 0 & 0
 \end{array} \right) & & \\
 \vdots & & & & & & \\
 O + \tilde{N}_r & & & & & & \\
 \vdots & & & & & & \\
 O + \tilde{N}_r + \tilde{N}_s & & & & & &
 \end{matrix}$$

Our simulator is based on OMNeT++¹ and uses the communication network package inet with extensions for WiFi EDCA, TDM/WDM PONs, and integrated WLAN-PON routing. The PON part is implemented corresponding to conventional EPON point-to-multipoint communications with REPORT-GRANT control messages. As for the WLAN EDCA-based network, a finite state machine model is developed and available in the inet² package, which includes the main IEEE 802.11e states such as *idle*, *defer*, *wait-AIFS*, *back-off*, *wait-ack*, *receive-ack*, *wait-SIFS*, and *receive*. Furthermore, we developed the probabilistic analysis calculator in Python using the scientific computing package NumPy³.

¹The open source simulator OMNeT++ is available at <http://www.omnetpp.org/>.

²The INET framework is available at <http://inet.omnetpp.org/>.

³For more information on NumPy please refer to <http://www.numpy.org/>.

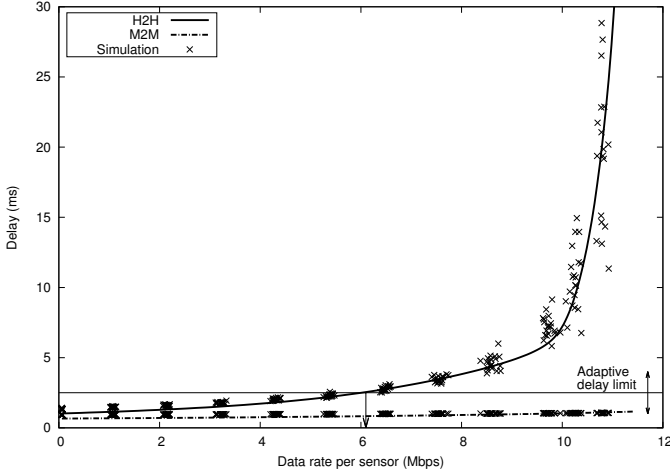


Fig. 4. Average end-to-end delay performance vs. data rate per sensor (event-driven sensors based on IEEE 802.11n).

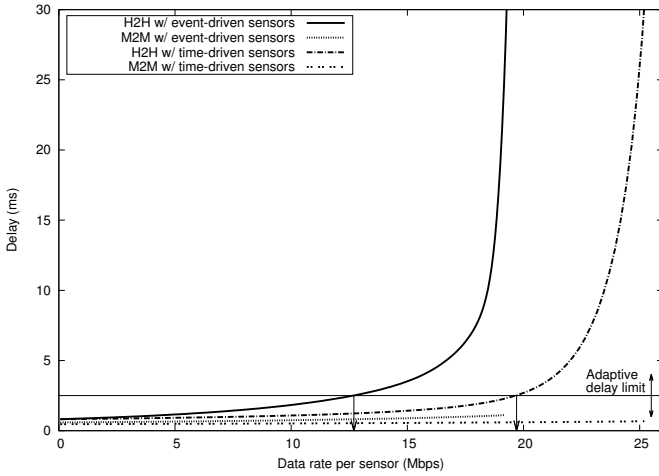


Fig. 5. Average end-to-end delay performance vs. data rate per sensor (time- and event-driven sensors based on IEEE 802.11ac).

B. Reliability and Maximum M2M Traffic Rate with a Conventional TDM EPON

We first consider a 20 km long TDM EPON with 8 ONUs, each equipped with an AP serving 2 STAs and 2 sensors.

Figs. 4 and 5 depict the average end-to-end delay performance of H2H traffic (aggregate load fixed to 144 Mb/s) and M2M sensor traffic vs. data rate per sensor. Fig. 4 shows the comparison between M2M and H2H traffic based on event-driven sensors and IEEE 802.11n, respectively. We observe from the figure that analytical and simulation results match closely. Note that the delay of M2M traffic remains low and flat for event- and especially time-driven sensors due to its smaller $\delta_{k,c}$ and CW_{min} . However, for increasing sensor data rates, the delay of H2H traffic may cross a given upper delay limit, which is adaptive to meet different H2H traffic requirements. For instance, for an upper delay limit of 2.5 ms, the measured sensor data rates of 6.1, 12.7, and 19.7 Mb/s (vertical arrows in Figs. 4-5) clearly show that higher permissible sensor data rates can be achieved by using VHT

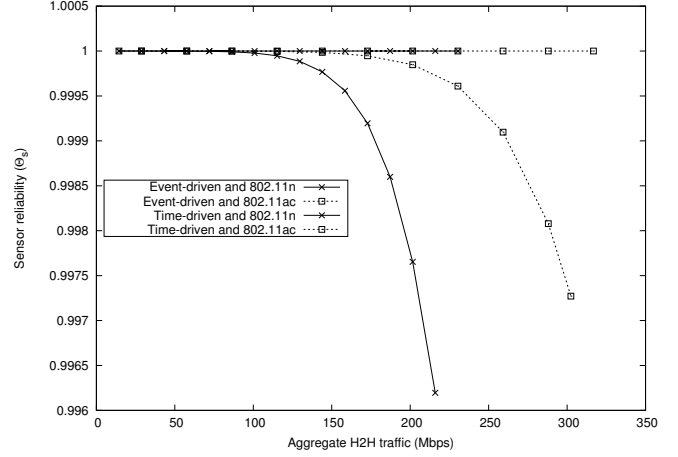


Fig. 6. Sensor reliability performance vs. aggregate H2H traffic load.

WLAN (IEEE 802.11ac) based event- or even better time-driven sensors instead of 802.11n based ones without violating the delay limit.

Fig. 6 shows the sensor reliability vs. aggregate H2H traffic under the assumption that each sensor generates 350 packets per second. We observe that time-driven sensor traffic is completely unaffected by increasing H2H traffic due to the lack of contention and packet collisions. In contrast, the reliability of event-driven sensor traffic drops sharply for increasing H2H traffic, in particular for lower-rate 802.11n based sensors due to their higher probability of packet collisions.

C. Triple-play and Smart Grid Traffic Settings

To consider more realistic traffic scenarios in the following result sections, we use the average payload lengths obtained from traffic measurements of smart grid applications based on IEC 61850 [14].

TABLE II
EXPERIMENTAL MEASUREMENTS OF SMART GRID MONITORING APPLICATIONS BASED ON IEC STANDARD 61850.

Source node	Average payload length
HVA/LV	500 bytes
Substation	5000 bytes
DER	224 bytes
Switch	100 bytes

We consider two traffic classes: one regular class for triple-play (e.g., voice, video, and data) traffic and another one for smart grid monitoring traffic. We set the average payload length to 1500 octets, which corresponds to the maximum Ethernet payload length. For the monitoring traffic, the data rate of smart grid sensors is configurable. We captured the traffic of experimental telecontrol smart grid applications in [14]. The average payload length originating from different smart grid nodes, including high-voltage/low-voltage (HV/LV) transformers, substation, distributed energy resources (DERs), and controllable switches are presented in Table II. Note that a single variable-value pair (following the format of manufacturing message specification messages (MMSs) of

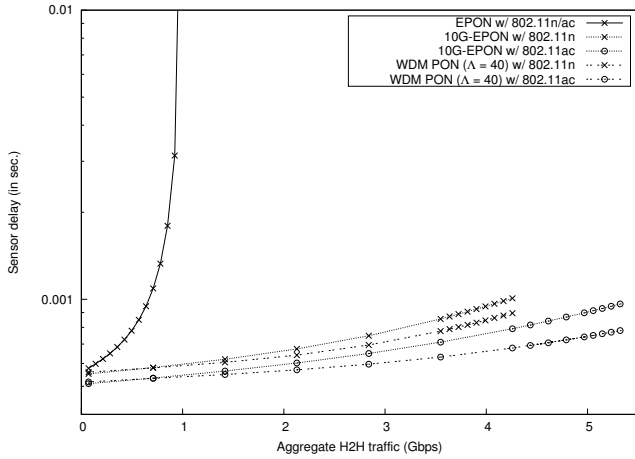


Fig. 7. Impact of H2H traffic loads on sensor delay.

IEC 61850) corresponds to 100 bytes. The measured payload length of 500 bytes for the HV/LV nodes, used in the following for the smart grid traffic, corresponds to active/reactive power, voltage, current, and location messages.

Using these settings, we set the average payload length \bar{L} and mean variance accordingly in the analytical framework to obtain the following results in Sections IV-D and IV-E.

D. Impact of Varying H2H Traffic for Different PON Types

We next consider larger TDM/WDM PONs consisting of 128 ONUs with 2 event-based sensors and 2 STAs per ONU. Each sensor generates $\lambda_{i,c}^{wi} = 10$ frames of 500 bytes per second. As H2H traffic is bursty and may significantly vary over time, it not only has an impact on H2H average delay but also affects M2M end-to-end delay.

The average end-to-end delay of event-driven sensors at different H2H traffic loads and PON types is depicted in Fig. 7. Note that the figure shows the end-to-end delay under varying H2H traffic loads, whereby the experienced H2H traffic delay is smaller than a given threshold of 2.5 ms. Specifically, with a conventional TDM EPON operating at 1 Gbps, the threshold of 2.5 ms of the H2H traffic delay is reached at an aggregate H2H traffic load of 1 Gbps, whereby the high traffic intensity of the PON affects both H2H and M2M traffic classes.

When upgrading the TDM EPON to a 10G-EPON or 40 Gbps WDM PON, we observe from Fig. 7 that the sensor delay performance is not significantly affected at any H2H traffic load, whereby the end-to-end delay remains below the threshold. In fact, the system bottleneck in this case is at the STAs, which become saturated without affecting the event-driven sensors. Note that upgrading the wireless nodes from 802.11n (capacity: 300 Mbps per zone) to 802.11ac (capacity: 6900 Mbps per zone) helps increase the H2H traffic load by only 1 Gbps for the considered configurations due to the low efficiency of the wireless MAC protocol.

E. Sensibility Analysis of Interplay Between Time- and Event-driven Nodes

We next analyze the interplay between time- and event-driven nodes. To do so, we vary the number of H2H and M2M nodes and find the theoretical upper bound of M2M traffic by using Eq. (37), as listed in Table III. The overall H2H aggregate load is fixed to 500 Mbps and event-driven nodes are based on IEEE 802.11n.

TABLE III
THEORETICAL UPPER BOUNDS (IN MBPS) OF M2M TRAFFIC FOR A GIVEN H2H DELAY THRESHOLD OF 2.5 MS

	Sensors per ONU $\left(\frac{\bar{N}_s}{O}\right)$							
	time-driven				event-driven			
	1	2	3	4	1	2	3	4
$\frac{\bar{N}_r}{O} = 1$	67.2	33.6	22.4	16.8	25.4	8.0	4.6	3.3
$\frac{\bar{N}_r}{O} = 2$	66.9	33.5	22.3	16.7	18.8	6.5	3.9	2.8
$\frac{\bar{N}_r}{O} = 3$	66.9	33.5	22.3	16.7	16.6	6.0	3.6	2.5
$\frac{\bar{N}_r}{O} = 4$	67.1	33.55	22.37	16.78	15.2	5.6	3.4	2.4

In Table III, the upper bound for all permutations of [1, 2, 3, 4] STAs/ONU and [1, 2, 3, 4] sensors/ONU is computed to study their impact on the theoretical upper bound. In the case of time-driven sensors, the behavior is expectedly linear, whereby the theoretical upper bound of M2M traffic depends on the number of time-driven nodes. However, in the case of event-driven sensors, the linear behavior is not observed. As the EDCA priority of STAs is low, the theoretical upper bound decreases nonlinearly as a function of the number of event-driven nodes (STAs and sensors). For instance, with 2 event-driven sensors and 1 STA, $2 \cdot 8 \text{ Mbps} = 16 \text{ Mbps}$ is obtained for both sensors (and $4 \cdot 3.3 = 13.2 \text{ Mbps}$ for 4 event-driven nodes), which is lower than in the case of 1 event-driven sensor (25.4 Mbps). We also note that the number of event-driven sensors (columns event-driven 1 to 4 in Table III) has a significantly stronger impact on the theoretical upper bound than the number of STAs (rows $\frac{\bar{N}_r}{O} = 1$ to $\frac{\bar{N}_r}{O} = 4$ in Table III) for the considered scenarios.

V. CONCLUSIONS

Recently, we developed the first unified analytical framework for the throughput-delay performance evaluation of arbitrary FiWi network routing algorithms [11]. In this paper, we extended our previous analytical framework for emerging multi-tier integrated FiWi smart grid communications infrastructures, which allows us to find the theoretical upper bound of sensor M2M traffic coexisting with conventional H2H traffic, taking into account both event- and time-driven wireless sensors as well as regular wireless stations. The obtained results showed that with a conventional EPON the permissible data rates of event- and time-driven sensors can be as high as 12.7 Mb/s and 19.7 Mb/s, respectively, without violating a given H2H delay limit of 2.5 ms. Furthermore, sensor reliability in terms of successful packet rate drops sharply for event-driven sensors, while time-driven sensor traffic is unaffected by

increasing H2H traffic. Using experimental measurements of real-world telecontrol smart grid applications, we studied the impact of variable H2H traffic loads on the sensor delays. We found, with the considered configurations, that a conventional EPON can cause the bottleneck and increase the delay for both H2H and M2M traffic, while with 10G-EPON and WDM PON the bottleneck was located in the wireless network, thus depicting future challenges to combine both fiber and wireless networks efficiently. We also studied the interplay between time- and event-driven nodes. We found, with time-driven sensors, that the theoretical upper bound of M2M traffic is linearly dependent on the number of nodes, while with event-driven sensors the upper bound decreases nonlinearly more significantly compared with time-driven sensors.

REFERENCES

- [1] V. C. Gungor, D. Sahin, T. Kocak, S. Ergut, C. Buccella, C. Cecati, and G. P. Hancke, "A Survey on Smart Grid Potential Applications and Communication Requirements," *IEEE Transactions on Industrial Informatics*, vol. 9, no. 1, pp. 28–42, Feb. 2013.
- [2] V. K. Sood, D. Fischer, J. M. Eklund, and T. Brown, "Developing a Communication Infrastructure for the Smart Grid," in *Proc., IEEE Electrical Power & Energy Conference*, Montréal, QC, Canada, Oct. 2009, pp. 1–7.
- [3] G. Kramer, M. De Andrade, R. Roy, and P. Chowdhury, "Evolution of Optical Access Networks: Architectures and Capacity Upgrades," *Proceedings of the IEEE*, vol. 100, no. 5, pp. 1188–1196, May 2012.
- [4] "FTTH: Double Squeeze of Incumbents – Forced to Partner?" Arthur D. Little, 2010.
- [5] M. Tahon, J. V. Ooteghem, K. Casier, L. Deschuttere, S. Verbrugge, D. Colle, M. Pickavet, and P. Demeester, "Cost allocation model for a synergetic cooperation in the rollout of telecom and utility networks," in *Proc., Conference on Telecommunications Internet and Media Techno-Economics (CTTE)*, May 2011, Paper S3-2.
- [6] F. R. Yu, P. Zhang, W. Xiao, and P. Choudhury, "Communication Systems for Grid Integration of Renewable Energy Resources," *IEEE Network*, vol. 25, no. 5, pp. 22–29, Sep. 2011.
- [7] K. Moslehi and R. Kumar, "Smart Grid - A Reliability Perspective," in *Proc., Innovative Smart Grid Technologies*, Jan. 2010, pp. 1–8.
- [8] S. Tozlu, M. Senel, W. Mao, and A. Keshavarzian, "Wi-Fi Enabled Sensors for Internet of Things: A Practical Perspective," *IEEE Communications Magazine*, vol. 50, no. 6, pp. 134–143, Jun. 2012.
- [9] P. Yi, A. Iwayemi, and C. Zhou, "Developing ZigBee Deployment Guideline Under WiFi Interference for Smart Grid Applications," *IEEE Transactions on Smart Grid*, vol. 2, no. 1, pp. 110–120, Mar. 2011.
- [10] S. Rickers, C. Spiegel, G. Bruck, P. Jung, R. Lee, S. Park, and J. Yu, "Multi Data Rate Signaling based on IEEE 802.15.4," in *Proc., International Symposium on Applied Sciences in Biomedical and Communication Technologies*, Nov. 2010, pp. 1–4.
- [11] F. Aurzada, M. Lévesque, M. Maier, and M. Reisslein, "FiWi Access Networks Based on Next-Generation PON and Gigabit-Class WLAN Technologies: A Capacity and Delay Analysis," *IEEE/ACM Transactions on Networking (Early Access)*.
- [12] I. Tinnirello and G. Bianchi, "Rethinking the IEEE 802.11e EDCA Performance Modeling Methodology," *IEEE/ACM Transactions on Networking*, vol. 18, no. 2, pp. 540–553, Apr. 2010.
- [13] G. Bianchi, "Performance Analysis of the IEEE 802.11 Distributed Coordination Function," *IEEE Journal on Selected Areas in Communications*, vol. 18, no. 3, pp. 535–547, Mar. 2000.
- [14] M. Lévesque and M. Maier, "Probabilistic Availability Quantification of PON and WiMAX Based FiWi Access Networks for Future Smart Grid Applications," *IEEE Transactions on Communications*, vol. 62, no. 12, pp. 1958–1969, Jun. 2014.

PLACE
PHOTO
HERE

Martin Lévesque received his M.Sc. in Computer Science from UQAM, Québec, Canada in 2010. He then obtained his Ph.D. degree in Telecommunications from INRS, Université du Québec, in 2014. During summer 2013, he was a visiting scholar at EDF R&D in Clamart, France, where he researched on advanced smart grid multi-simulations. He was recipient of master and doctoral scholarships while pursuing his graduate studies. He served as a reviewer of numerous major journals and is a member of the IEEE IES Technical Committee on Smart Grids. He is currently a Postdoctoral Researcher with University of Pittsburgh, Pittsburgh, PA, funded by the prestigious Postdoctoral Fellowship program from the Natural Sciences and Engineering Research Council of Canada (NSERC).

PLACE
PHOTO
HERE

Frank Aurzada studied mathematics at the University of Jena, Jena, Germany, and the University of York, York, U.K. He received the Dipl.-Math. and Ph.D. degrees in mathematics from the University of Jena in 2003 and 2006, respectively. He was a Postdoctoral Researcher with TU Berlin, Berlin, Germany, from 2006 to 2012 and an Associate Professor with TU Braunschweig, Braunschweig, Germany, from 2012 to 2013. Since 2013, he has been a Professor with the Technical University Darmstadt, Darmstadt, Germany.

PLACE
PHOTO
HERE

Martin Maier is a Full Professor with the Institut National de la Recherche Scientifique (INRS), Montréal. He has joined INRS as an Associate Professor in May 2005. He received the MSc and PhD degrees both with distinctions (summa cum laude) in electrical engineering from the Technical University Berlin, Berlin, Germany, in 1998 and 2003, respectively. He was a Visiting Researcher at the University of Southern California (USC), Los Angeles, CA, in spring 1998 and Arizona State University (ASU), Tempe, AZ, in winter 2001. In summer 2003, he was a Postdoc Fellow at the Massachusetts Institute of Technology (MIT), Cambridge, MA. Before joining INRS, Dr. Maier was a Research Associate at CTTC, Barcelona, Spain, November 2003 through March 2005. He was a Visiting Professor at Stanford University, Stanford, CA, October 2006 through March 2007. Dr. Maier was a recipient of the two-year Deutsche Telekom doctoral scholarship from June 1999 through May 2001. He is also a co-recipient of the 2009 IEEE Communications Society Best Tutorial Paper Award and the Best Paper Award presented at The International Society of Optical Engineers (SPIE) Photonics East 2000-Terabit Optical Networking Conference. He served on the Technical Program Committees of IEEE INFOCOM, IEEE GLOBECOM, and IEEE ICC, and is an Editorial Board member of the IEEE Communications Surveys and Tutorials as well as ELSEVIER Computer Communications. He is a Senior Member of IEEE.

PLACE
PHOTO
HERE

Géza Joós received the M.Eng. and Ph.D. degrees from McGill University, Montreal, QC, Canada. He has been a Professor in the Department of Electrical and Computer Engineering Department at McGill University since 2001. He holds an NSERC/Hydro-Quebec Industrial Research Chair on the Integration of Renewable Energies and Distributed Generation into the Electric Distribution Grid (since 2009) and a Canada Research Chair in Intelligent Distribution Systems (since 2011). His research interests are in distributed generation and renewable energy, advanced distribution systems and microgrids. He was previously with ABB, the Université du Québec and Concordia University. He has consulting experience in the areas of power electronic converters, with applications to power systems, and power system planning and operation. Dr. Joós is active in working groups of the International Council on Large Electric Systems (CIGRE), dealing with distribution systems and distributed generation, and of the IEEE Power and Energy Society, dealing with power electronic applications to power systems. He is a Fellow of the Canadian Academy of Engineering and of the Engineering Institute of Canada.